nature COMMUNICATIONS

ARTICLE

Received 23 May 2013 | Accepted 14 Oct 2013 | Published 8 Nov 2013

DOI: 10.1038/ncomms3758

Carbon isotope records reveal precise timing of enhanced Southern Ocean upwelling during the last deglaciation

Giuseppe Siani[1], Elisabeth Michel[2], Ricardo De Pol-Holz[3], Tim DeVries[4], Frank Lamy[5], Mélanie Carel[1], Gulay Isguder[2], Fabien Dewilde[2] & Anna Lourantou[2,6]

The Southern Ocean plays a prominent role in the Earth's climate and carbon cycle. Changes in the Southern Ocean circulation may have regulated the release of CO_2 to the atmosphere from a deep-ocean reservoir during the last deglaciation. However, the path and exact timing of this deglacial CO_2 release are still under debate. Here we present measurements of deglacial surface reservoir ^{14}C age changes in the eastern Pacific sector of the Southern Ocean, obtained by ^{14}C dating of tephra deposited over the marine and terrestrial regions. These results, along with records of foraminifera benthic–planktic ^{14}C age and $\delta^{13}C$ difference, provide evidence for three periods of enhanced upwelling in the Southern Ocean during the last deglaciation, supporting the hypothesis that Southern Ocean upwelling contributed to the deglacial rise in atmospheric CO_2. These independently dated marine records suggest synchronous changes in the Southern Ocean circulation and Antarctic climate during the last deglaciation.

[1] Laboratoire des Interactions et Dynamique des Environnements de Surface (IDES), UMR 8148, CNRS-Université de Paris-Sud, Bâtiment 504, 91405 Orsay Cedex, France. [2] Laboratoire des Sciences du Climat et de l'Environnement (LSCE), Laboratoire mixte CNRS-CEA, Avenue de la Terrasse, 91198 Gif-sur-Yvette Cedex, France. [3] Department of Oceanography, Center for Climate and Resilence Research, University of Concepcion, Casilla 160-C, 4070386 Concepcion, Chile. [4] Department of Atmospheric and Oceanic Sciences, University of California, Los Angeles, California 90095, USA. [5] Alfred Wegener Institut fur Polar und Meeresforschung, Am Alten Hafen 26, 27568 Bremerhaven, Germany. [6] LOCEAN, Université Pierre et Marie Curie Paris VI, 4 place Jussieu, 75015 Paris, France. Correspondence and requests for materials should be addressed to G.S. (email: giuseppe.siani@u-psud.fr).

Knowledge of marine surface reservoir radiocarbon ages (R_{surf}, that is, the difference between the ^{14}C age of the sea surface and that of the atmosphere) allows the accurate correlation of continental, cryospheric and marine palaeoclimate records. Accurate comparison of palaeoclimate records is essential in order to understand the timing, causality and mechanisms of past climate changes. Besides enhancing the accuracy of age models, R_{surf} reconstructions also provide clues about past changes in ocean circulation patterns[1–3], some of which have been linked to the rise in atmospheric CO_2 over the last deglaciation[4–8]. In this respect, the Southern Ocean (SO), which connects the deep ocean with surface waters and the atmosphere, plays a major role in global ocean circulation and the carbon cycle[4,9]. It has been proposed that SO upwelling, the intensity of which depends partly on changes in the strength and position of Southern Hemisphere westerly winds, could be the primary route for ocean CO_2 degassing during the last deglaciation[4–8,10–13]. This so-called SO upwelling hypothesis remains a controversial issue. On one hand, records from intermediate depths in the South East Pacific (SEP) have shown a reduction in Antarctic Intermediate Water (AAIW) oxygen concentration during the deglacial warming period, which may be linked with an upwelling of low oxygen waters at the SO divergence, which are transported northward via AAIW[14]. On the other hand, ^{14}C records from the South Pacific do not indicate any deglacial ^{14}C depletion at intermediate depths off Chile and New Zealand[11,13], which does not support the SO upwelling hypothesis.

Part of the controversy may arise from potentially biased chronologies in marine sediment cores for which it is difficult to derive robust estimates of R_{surf}. Only one study has provided independent R_{surf} in the southwest Pacific Ocean[3] during the glacial period; however, there are no estimates for the SO during the deglaciation. Deep-sea coral records can provide robust chronologies for deep waters because of the direct comparison between U/Th and ^{14}C ages; however, they do not ensure a simultaneous climatic record for bottom and surface waters[15]. The precise dating of SO ventilation records is, however, crucial in linking CO_2 outgassing events, and their timing, to changes in atmospheric CO_2 concentrations recorded in ice cores.

Here we present the first deglacial Pacific SO record of R_{surf} based on the occurrence of tephra layers independently dated in the ocean and on land. The well-dated marine tephra used in this study is identified in the sediment core MD07-3088 collected off the southern Chilean margin (North Patagonia) at a depth of 1,536 m (Fig. 1). The core is located within the Antarctic Circumpolar Current (ACC) under the direct influence of the northward Ekman transport of Sub-Antarctic Surface Waters (SSW)[16] (Fig. 1a,b). Today, the core depth is bathed by the upper layers of the nutrient-rich, oxygen-poor Pacific Central Waters at the boundary with the northward-flowing oxygen-rich AAIW. Thus, this core is well located to monitor the past SO upwelling history. We show that R_{surf} at this location is larger during the deglaciation than during the Holocene and that periods of increased R_{surf} are coeval with periods of increased SO vertical mixing. These precisely dated palaeoceanographic records indicate a strong correlation between SO upwelling events and the deglacial atmospheric CO_2 rise, providing strong support for the SO upwelling hypothesis. The R_{surf} reconstructions also help to reveal a deglacial ageing of AAIW that is consistent with its reduction in oxygen concentration[14], indicating that deglacial CO_2 excess was spread, at least partly, via an AAIW pathway.

Results

Climatic record in core MD07-3088. Climatic conditions of surface waters at core MD07-3088 are recorded in the stable oxygen isotopes ($\delta^{18}O$) of planktonic foraminifera *Globigerina bulloides* (Fig. 2a) and the summer sea–surface temperature (SST), obtained by planktonic foraminifera assemblages and the Modern Analogue Technique (Fig. 2b). The $\delta^{18}O$ and SST records show variations characteristic of the last glacial/interglacial transition and the Holocene, with two warming phases (W1 and W2) separated by a reversal to colder conditions (Oceanic Cold Reversal or OCR) (Fig. 2). Both the $\delta^{18}O$ and SST records display short-term variability within each climatic phase, potentially indicating abrupt hydrographic changes.

Radiocarbon ages and stable carbon isotopes. R_{surf} estimates are based on detailed geochemical analyses and ^{14}C dating of both terrestrial and marine tephra deposits (Supplementary Table S1; Fig. 2e). Over the last deglaciation, five tephra showed that R_{surf} was at 1,320 ± 95 years at the end of the first phase of deglacial warming (W1 on Fig. 2, HW1 tephra). R_{surf} decreased to 975 ± 120 years during the OCR (HW2 tephra), to 920 ± 135 years during the second warming phase (W2 on Fig. 2, HW3 tephra) and to 800 years during the Holocene (H2 and HW7 tephra; Fig. 2e).

Today, pre-bomb R_{surf} is poorly documented in the SEP, except for one single available date at 530 ± 40 years from the southern Chilean fjords (51 °S, 72 °E (ref. 17)). This fjord site is not likely to be representative of open ocean conditions, as it is largely affected by local conditions such as melt-water supply[18]. Our results indicate that the youngest R_{surf} estimates at *ca.* 800 years, obtained from core MD07-3088 during the upper Holocene, are similar to those obtained during the Middle Holocene and are in agreement with other studies carried out along the SEP margin, as well in the SO, which have revealed no changes in regional R_{surf} during this period[19–22]. As a consequence, middle to upper Holocene R_{surf} estimate at *ca.* 800 years along the Southern Chilean margin at 46 °S can be regarded as the most plausible for the pre-bomb period.

We assume that the large R_{surf} changes during the deglacial period in core MD07-3088 cannot be because of contamination by old carbon carried by the Aisén and northern Patagonian tributary rivers, as the main geological units of the Coastal Range and Cordillera are composed primarily of pre-Jurassic metamorphic basement, ophiolite, plutonic rocks and volcanic material[23]. This assumption is supported by the $\delta^{18}O$ and $\delta^{13}C$ records of the planktic foraminifera *G. bulloides* from MD07-3088 and a farther offshore core, MD07-3119 (46°05 S, 76°06 W, 2,520 m), recovered at the same latitude (Supplementary Fig. S1). The results show similar $\delta^{18}O$ and $\delta^{13}C$ oscillations during the deglaciation and early Holocene, clearly indicating that the core MD07-3088 signals are representative of the open ocean and are not influenced by local coastal effects.

R_{surf} changes can result from changes in the atmospheric ^{14}C activity or from variations in the exchange of surface waters with the atmosphere and underlying ^{14}C-depleted waters. Variability in vertical mixing (stratification) is effectively recorded in differences between the carbon isotope composition of benthic and planktonic foraminifera (B-P ^{14}C age and $\Delta\delta^{13}C$). We evaluate the influence of changing atmospheric ^{14}C activity on B-P ages using an ocean circulation model (see Methods).

B-P age differences were ~1,400 ^{14}C years during the Late Glacial, ~400 years higher than modern values (modern B-P is ~1,000 years[24]), suggesting more stratification and poorly ventilated deep-water masses in the SEP region (Fig. 2c; Supplementary Table S2). The late glacial–interglacial transition is marked by three periods of low values for B-P age, coeval with three periods of low $\Delta\delta^{13}C$ values (Fig. 2d). The end of the first short decrease in the B-P age and $\Delta\delta^{13}C$ marks the onset of the

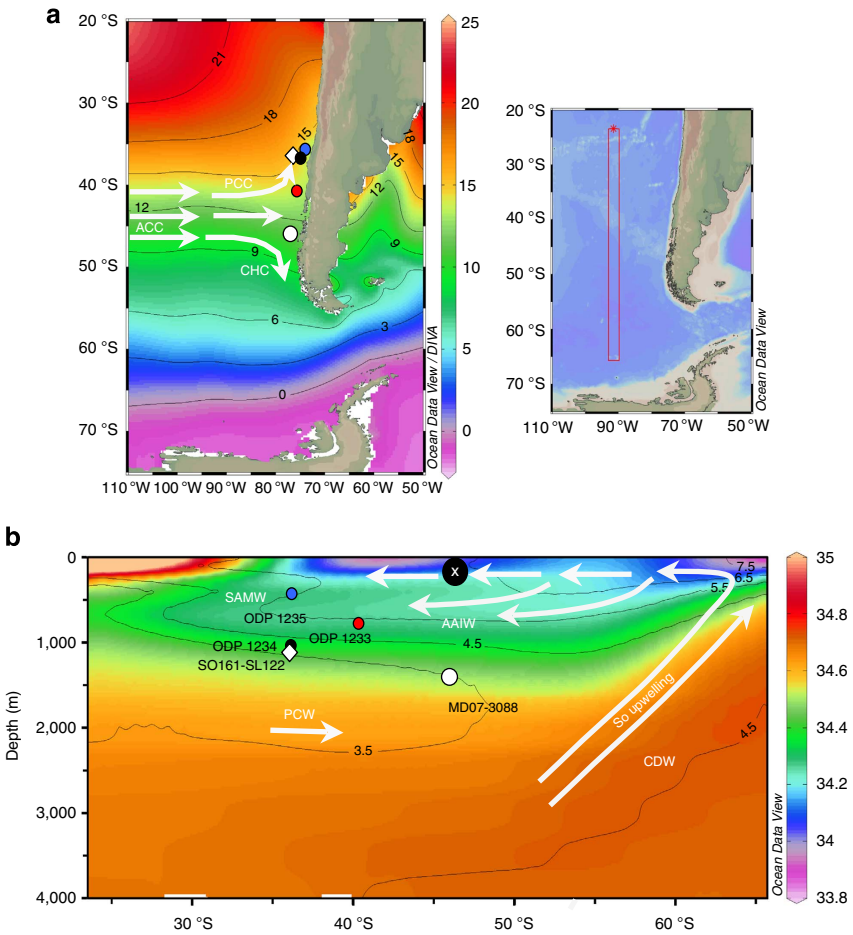

Figure 1 | Study area and core locations. (**a**) Map of the mean annual SST (°C) using the Ocean Data View (ODV) software[56] and geographical locations of cores MD07-3088 (46 °S, 75 °W, 1,536 m; white circle), ODP 1233 (41 °S, 74 W, 838 m; solid red circles[14]), ODP 1234 (36 °S, 73 °W, 1,015 m; solid black circles[14]), ODP 1235 (36 °S, 73 °W, 489 m; solid blue circles[14]), and SO161-SL122 (36 °S, 73 °W, 1,000 m; white diamond[11]). ACC: Antarctic Circumpolar Current. PCC: Peru–Chile Current. CHC: Cape Horn Current. The inset on the map corresponds to the transect for the latitude-depth section presented in **b**. (**b**) Salinity (psu, coloured shading) and oxygen (ml l^{-1}, thin black contours) depth-latitude section. SAMW: Sub-Antarctic Mode Waters. AAIW: Antarctic Intermediate Water. PCW: Pacific Central Water. CDW: Circumpolar Deep Water. The filled circle with cross indicates the flow of SSW. Core location is indicatively plotted following the inset of Fig. 1a at the same collected depth and latitude but at different longitude.

deglaciation, followed by two longer periods of low values. During the first warming episode W1, the B-P age reaches its minimum value of 450 years. Then, B-P age and $\Delta\delta^{13}C$ increase during the OCR, prior to a third period of low values during the second warming W2 (Fig. 2c,d). Thus, the oldest R_{surf}, at 1,320 ± 95 years, which occurred during the minima of the B-P age within the episode W1, could originate from enhanced upwelling of ^{14}C-depleted deep waters.

Age model and mechanisms for R_{surf} changes. To establish the chronology of the core, we used 24 ^{14}C ages on planktic foraminifera corrected with the R_{surf} age determined from the tephra layers (Fig. 2f). Then, the R_{surf}-corrected planktic ^{14}C dates were calibrated using the OxCal software[25] based on the IntCal09 (ref. 26) calibration curve. We also present most of the results using the IntCal04 (ref. 27) calibration curve as it critically deviates from IntCal09 during 17.5 to 15 ka BP, in line with recent nonmarine data from speleothems[28] and varved lake sediments[29]. ^{14}C data and R_{surf} estimates are reported in Supplementary Tables S1,S2.

Prior to the HW1 tephra, marine ash layers found in the core could not be correlated to dated terrestrial volcanic products[30]. To date, existing continental records west of the Andes do not extend beyond 15 ka because of the presence of a permanent icecap in the region[31]. Before 14.5 ka, we apply the basic assumption of using the highest R_{surf} (1,320 years from the HW1 tephra) when the B-P age and $\Delta\delta^{13}C$ decrease (Fig. 2), and the lowest R_{surf} (800 years from the H2 and HW7 tephra) for times when the B-P age and $\Delta\delta^{13}C$ are relatively constant. This approach is based on the observation that the major R_{surf} increase in core MD07-3088, which occurred during the last deglaciation, is contemporaneous with the maximum decrease in B-P age difference, suggesting mixing with ^{14}C-depleted deep waters. The B-P age difference during the last glaciation is noticeably higher than that during the deglacial period, indicating well-stratified water masses and the fact that glacial atmospheric $\Delta^{14}C$ was higher. A well-stratified water mass could lead to a reduced R_{surf} during the late glacial period. However, it might have been compensated for by the higher glacial atmospheric $\Delta^{14}C$ and the reduced air–sea CO_2 flux because of lower pCO_2. Therefore, we assume that R_{surf} during the last glaciation did not differ significantly from that of the Holocene period.

The inferred decrease in the B-P age and $\Delta\delta^{13}C$ variations (Fig. 3a,b) originate either from enhanced vertical mixing in the SO (as for the HW1–HW2 period when R_{surf} shows an opposite

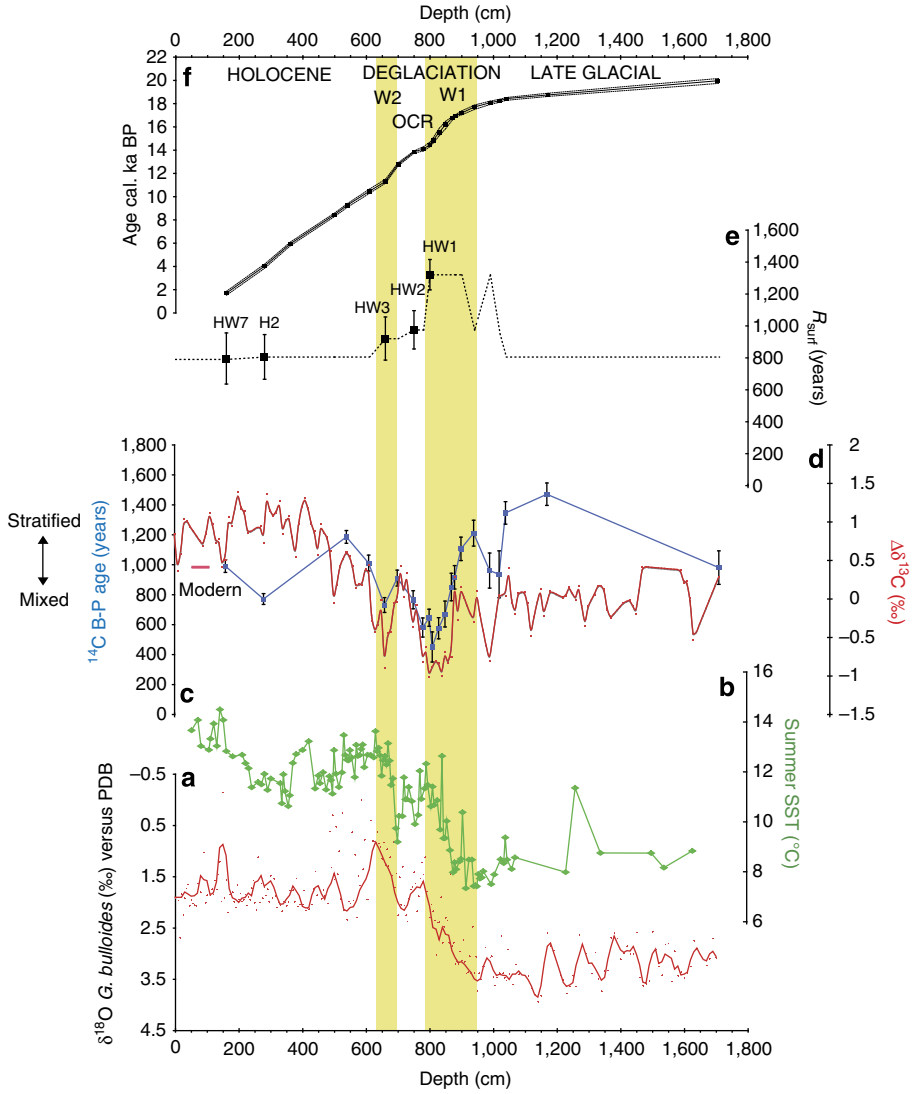

Figure 2 | Records and age control of core MD07-3088. (**a**) δ^{18}O (per mil versus PDB) of *G. bulloides*. Smoothed curve using a three-point average (thick red line). (**b**) Summer Sea Surface Temperature (°C) using Modern Analogue Technique. (**c**) ^{14}C age difference between paired benthic and planktic foraminifera (^{14}C B-P; filled squares). The error bars represent combined error at 1. Red dash: modern B-P ^{14}C age[24]. Double-ended arrow indicates stratified (higher ^{14}C B-P and $\Delta\delta^{13}$C values) versus mixed (lower ^{14}C B-P and $\Delta\delta^{13}$C values) water mass. (**d**) $\Delta\delta^{13}C = \delta^{13}C$ *G. bulloides*—$\delta^{13}C$ *C. wuellerstörfii* (red dots). Smoothed curve using a three-point average (thick red line). (**e**) R_{surf} age (squares) and assumed R_{surf} (dotted line) in core MD07-3088. HW7, H2, HW3, HW2, HW1: terrestrial tephra from the Hudson volcano (Supplementary Table S1). The error bars represent combined error at 1σ. (**f**) Calibrated ^{14}C ages (ka BP) versus depth with 1σ uncertainties. OCR: Ocean Cold Reversal. W1 and W2 (yellow shading): the two Southern Ocean warming phases of the last deglaciation.

trend to the B-P age) or from rapid changes of the atmospheric δ^{13}C compositions. In the atmosphere, two decreases have been observed in the δ^{13}C signal[32,33] during the deglaciation (Fig. 3d); however, the amplitude of this atmospheric signal is only half that of the ocean surface δ^{13}C that we have measured (Fig. 3c). Similarly, we checked that rapid decreases in atmospheric Δ^{14}C (Fig. 3g (refs 27,28)) could not entirely explain the amplitude and timing of the decreases in the B-P age signal in core MD07-3088. The B-P age record, corrected for variations in atmospheric Δ^{14}C, is shown in Fig. 3a with the raw B-P ages (see Methods). The similarity between the raw and the corrected B-P ages indicates that both carbon isotopic signals mainly reflect changes in SO upwelling. Furthermore, the largest and longest period of low $\Delta\delta^{13}$C and B-P age difference is associated with the highest R_{surf} during the last deglaciation, emphasizing that SO upwelling provided a conduit for a ^{14}C-depleted deep-water mass to surface waters at that time (Fig. 3a,b,f). Conversely, during the OCR, a lowering of R_{surf} to ~1,000 years mirrors the rise in $\Delta\delta^{13}$C and B-P age, indicating weaker SO upwelling. However, during W2, the next period characterized by both a lower $\Delta\delta^{13}$C and a slightly lower B-P age difference, the observed R_{surf} changes vary little from their OCR value. Upwelled deep waters might have carried a much younger ^{14}C age during W2 than at the beginning of the deglaciation because of the first period of vertical convection in the SO and the resumption of deep-water formation in the North Atlantic after the Heinrich 1 event[34]. Another alternative is that the apparent B-P age decrease is because of variations in atmospheric Δ^{14}C, as indicated by the B-P age data corrected for atmospheric Δ^{14}C changes (Fig. 3a). One possible explanation for the apparent discrepancy in the R_{surf} and δ^{13}C records during W2 is that the production rate of ^{14}C in the atmosphere decreased during that time. If this were the case,

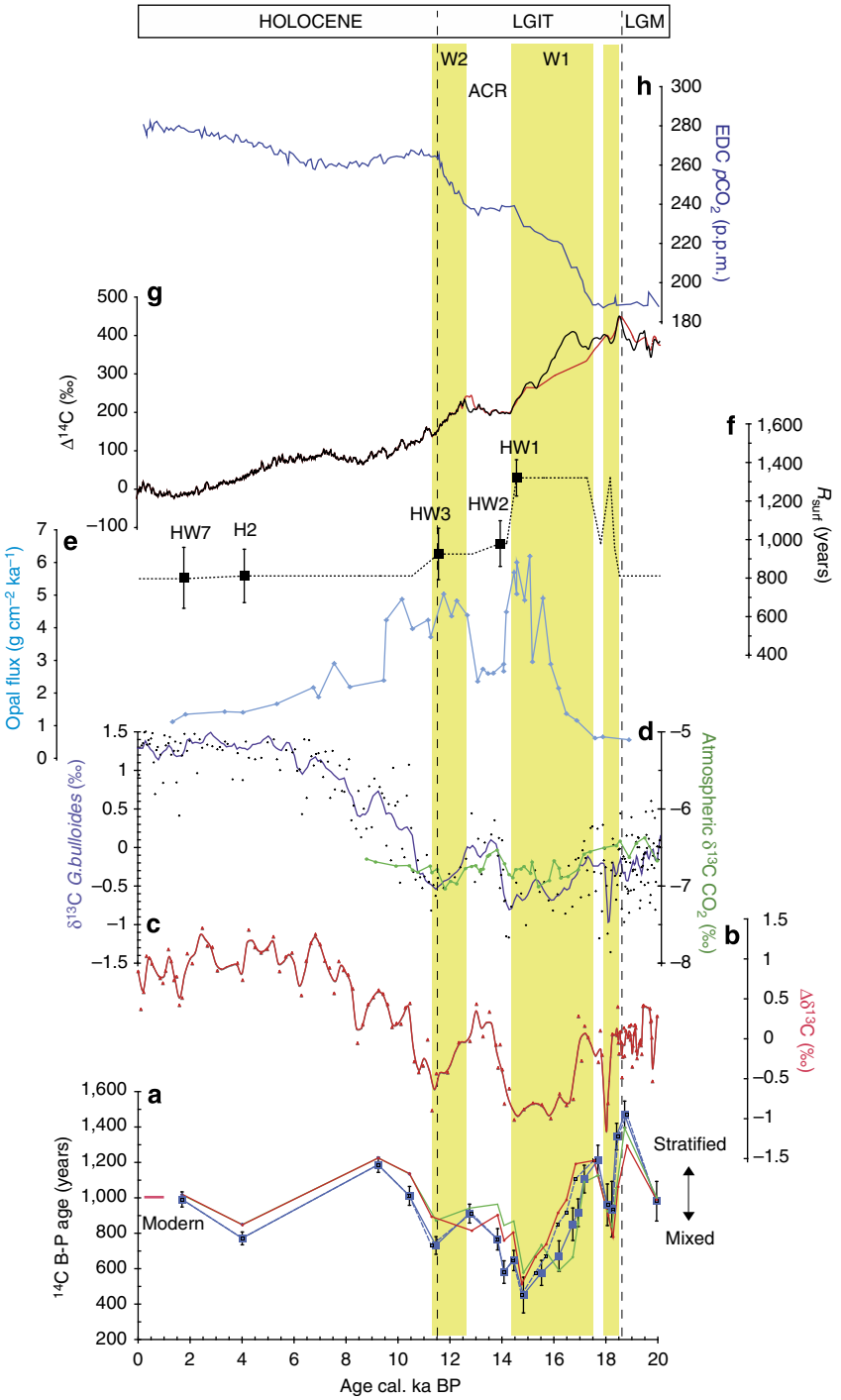

Figure 3 | Southern Ocean and atmospheric carbon cycle changes during the last deglaciation. (**a**) Paired benthic and planktic foraminifera radiocarbon age difference (^{14}C B-P age; this study) using IntCal09 (thick blue line) and IntCal04 (dashed blue line) versus time. The error bars represent combined 1σ error in the radiocarbon dates. The B-P age difference corrected for Δ^{14}C atmospheric changes (see Methods) is shown in red and green for IntCal04 and IntCal09, respectively. Double-ended arrow indicates stratified (higher B-P ^{14}C values) versus mixed (lower B-P ^{14}C values) water mass. Red dash: modern B-P ^{14}C age[24]. (**b**) $\Delta\delta^{13}$C in core MD07-3088; smoothed curve using a three-point average (thick red line). (**c**) *G. bulloides* δ^{13}C (this study); smoothed curve using a three-point average (thick purple line). (**d**) Ice core EDC $\delta^{13}CO_2$ measurements (green)[32] versus age scale from Lemieux-Dudon *et al.*[36] (**e**) Southern Ocean Opal flux, a proxy for upwelling south of the Antarctic polar front from core TN057-13-4PC (ref. 5). (**f**) R_{surf} (squares) and assumed R_{surf} (dotted line) in core MD07-3088. (**g**) Atmospheric ^{14}C activity (Δ^{14}C), IntCal09 (black line), IntCal04 (red line)[26,27]. (**h**) Atmospheric CO_2 from ice-core EDC[35]. The vertical grey dashed lines indicate the approximate timing of Southern Hemisphere climatic events. LGIT: Last Glacial/Interglacial transition; ACR: Antarctic Cold Reversal; LGM: Last Glacial Maximum. Yellow shaded area: the three phases of Southern Ocean outgassing. W1 and W2: the two Southern Ocean warming phases of the last deglaciation.

an increase in upwelling might not be recorded as an increase in R_{surf}. At the end of this third period of enhanced vertical mixing, R_{surf} decreases towards its Holocene value, which is similar to the modern.

Discussion

The reconstructed age model for core MD07-3088 makes it possible to compare the EPICA Dome C (EDC) and SEP climatic records. Figure 3 illustrates the MD07-3088 records on a calendar age (cal.) scale, compared with the atmospheric $\delta^{13}C$[35] and isotopic compositions from the EDC ice core[32,36] and the record of atmospheric ^{14}C activity[26,27]. The planktic foraminifera $\delta^{13}C$ record from core MD07-3088 shows a similar pattern to the $\delta^{13}C$ of CO_2 inferred from the EDC ice core (Fig. 3c,d (ref. 32)). The excellent synchronicity of both records is particularly well documented for the rapid $\delta^{13}C$ increase between 14.1 and 13.5 cal. ka BP in both our marine and the ice-core record. This event is chronologically very well constrained by two tephra, at 14.47 ± 0.2 and 13.76 ± 0.1 cal. ka BP, in our record and is synchronous with the $\delta^{13}C$ rise of CO_2 according to the recent chronology of the EDC ice-core record[36] within the 1σ uncertainties. Here, for the first time, we are able to demonstrate a good synchronicity between climatic marine and cryospheric records in the Southern Hemisphere for a rapid event, displaying high temporal resolution (<150 years) and accurately dated boundaries. In general, the first order, and most of the second order, changes in the marine $\delta^{13}C$ and $\delta^{18}O$ and SSST records match well with the EDC $\delta^{13}C$ and deuterium isotopic (δD) records during deglaciation (Figs 3,4). Interestingly, for the SEP, the OCR cold spell is coeval with the Antarctic Cold Reversal event within the 1σ uncertainties (Fig. 4a,b,d). Moreover, in the SEP we do not see a delay as large as 800 years between the Antarctic Cold Reversal and OCR event as suggested for the South Indian Ocean[37]. These results are corroborated by the good match between the high-resolution Ti/K record and the EDC deuterium isotopic (δD) record (Fig. 4c,d). The Ti/K ratio has been used as a proxy to track past changes in the relative contribution of the terrigenous source derived from the volcanic area (high contents of Ti-rich minerals) of the Andean Cordillera versus that derived from the igneous rocks (high contents of K-rich minerals) of the Coastal Range[38]. These environmental changes have been attributed to climate fluctuations that occurred since the last glacial period in northern Patagonia and have been mainly related to precipitation and glacier behaviour[38].

The two steps in atmospheric CO_2 increase during the deglaciation[35], from 17.4 to 14.4 ka and 12.5 to 11.5 ka, respectively[36], are synchronous with the two latest periods of SO upwelling, indicated both by the B-P age and $\Delta\delta^{13}C$ decrease in core MD07-3088 (Fig. 3h, shaded areas W1 and W2). The precise timing of these core records supports the hypothesis that ocean CO_2 outgassing through SO upwelling is a major mechanism responsible for the deglacial atmospheric CO_2 rise[4]. The first period of SO upwelling, starting at ~18.4 cal. ka BP (Fig. 3, shaded area), occurs at the very beginning of the deglaciation as indicated by planktic foraminifera $\delta^{18}O$ and by a recent composite record of Antarctic ice core temperatures[39]. This supports a coeval onset of Antarctic temperature and atmospheric CO_2 rise as suggested by recent studies on gas and ice-age difference of the ice cores[40,41].

The W1 and W2 upwelling periods identified in core MD07-3088 correspond to opal productivity events observed in the Atlantic and Pacific sectors of the SO (ref. 5) south of the polar front (core TN057-13-4PC; Fig. 3e). However, the deglacial SO opal flux record does not register enhanced opal productivity during the first short-term period of SO upwelling recorded in

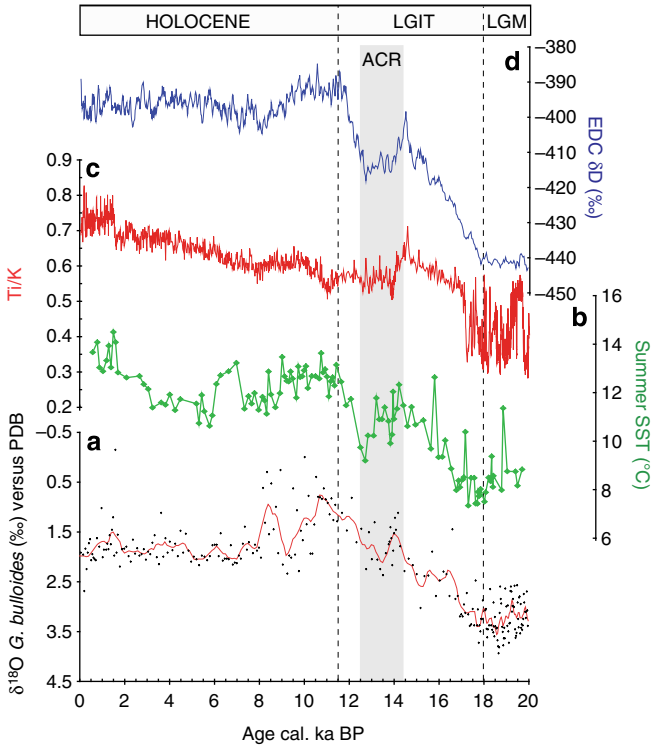

Figure 4 | Comparison of palaeoclimatic records from core MD07-3088 and EPICA DOME C. (**a**) Variations in $\delta^{18}O$ (per mil versus PDB) of *G. bulloides* versus time. The thick red line corresponds to a smoothed curve using a three-point average. (**b**) Summer SST (°C) using the Modern Analogue Technique. (**c**) Ti/K ratio sedimentary record in core MD07-3088. (**d**) Ice-core deuterium (δD) record from EDC[35] based on the age scale of Lemieux-Dudon *et al.*[36] Note that the calendar age scale of the marine records (**a**-**c**) was determined in this study from marine radiocarbon data and is independent of the calendar age scale for the ice-core record (**d**). Vertical grey dashed lines indicate approximate timing of Southern Hemisphere climatic events. LGM = Last Glacial Maximum, LGIT = Last Glacial–Interglacial transition; ACR = Antarctic Cold Reversal.

core MD07-3088 at ~18.4 cal. ka BP. There are two possible explanations for this. First, it could be that the sedimentation rate in core TN057-13-4PC is not high enough to record so rapid an event. Second, it could be that the location of maximum opal production at the end of the last glacial maximum was shifted further north of the sub-antarctic zone and is therefore not recorded in this core[4].

The three periods of SO upwelling correspond to three rapid decreases in atmospheric $\Delta^{14}C$ as indicated by the IntCal04 curve[27] (Fig. 3g). The major discrepancy between the IntCal09 (ref. 26) and IntCal04 (ref. 27) curves concerns the second deglacial event of SO upwelling. For this second event to be synchronous with the timing of the $\Delta^{14}C$ decrease in IntCal09 (~16.35 cal. ka BP), the R_{surf} should rise to up to $2{,}160 \pm 100$ years. However, with such an increase in R_{surf}, the second SO upwelling event would no longer be synchronous with the rapid CO_2 increase starting around 17.4 cal. ka BP (Fig. 3g). Moreover, the recently published complete terrestrial ^{14}C record for the 11.2–52.8 cal. ka BP interval[29] is more in agreement with the IntCal04 than the IntCal09 record.

The inferred R_{surf} changes outlined here enable us to reconcile several SEP marine palaeoceanographic studies at the regional scale and to clarify part of the controversy regarding the ventilation age history of AAIW.

A recent compilation of the B-P ^{14}C age difference between paired benthic and planktic foraminifera from the central Chile margin (Fig. 1; SO161-SL22; 36 °S, 73 °W; 1,000 m water depth; ref. 11) shows similar overall late Glacial to Holocene ventilation variations when compared with the MD07-3088 B-P record (Fig. 5a). However, the age models of the two cores differ, with regard to the onset of the deglacial B-P age decrease identified at ~18.8 cal. ka BP in core SO161-SL22. In fact, without information on potential changes in R_{surf}, De Pol-Holz *et al.*[11] assumed a constant R_{surf} of 400 years at site SO161-SL22 to establish the age model of the core. As shown above, the largest and longest period of the low B-P age difference in our record (between *ca.* 17 and 14 cal. ka BP) is associated with the highest observed R_{surf} in the SEP during the last deglaciation, emphasizing the mixing of upper intermediate and surface waters with a ^{14}C-depleted deep-water mass. On the basis of these observations, the existence of a B-P age phase shift between both records appears questionable. Today, the SO161-SL22 site is under the influence of the surficial Peru–Chile current originating from the northern branch of the ACC. Thus, surface waters at MD07-3088 and SO161-SL22 sites should have undergone similar R_{surf} changes.

By using a constant R_{surf} age of 400 years in their age model, De Pol-Holz *et al.*[11] reconstructed an age-corrected AAIW $\Delta^{14}C$ record displaying no significant depletion of the AAIW $\Delta^{14}C$ values and suggesting no mixing with any hypothetical ^{14}C-depleted deep-ocean reservoir during the Heinrich 1 and/or the Younger Dryas periods (Fig. 5b (ref. 11)). In contrast, the reconstructed $\Delta^{14}C$ values (at the lower boundary with AAIW) in the MD07-3088 record show a significant aging of these waters in the SEP at the onset of the deglaciation, which lasted until 16.7 cal. ka BP (Fig. 5b). In order to shed light on this point, we recalculated the $\Delta^{14}C$ record from the northern Chile margin core SO161-SL22, using the R_{surf} changes determined for MD07-3088. The derived ventilation ages are about twice as old as the original ones, revealing the degree to which unaccounted R_{surf} variability may affect $\Delta^{14}C$ calculations. This finding reveals an ageing of AAIW during the first deglacial warming (17.5–14.5 cal. ka BP) that is consistent with a reduction in the AAIW oxygen concentration at ocean drilling program (ODP) sites 1,233, 1,234 and 1,235 located at 41 °S and 36 °S, respectively (Fig. 1; (ref. 14)). The large difference between the ventilation age variations of AAIW calculated assuming a constant R_{surf}[11], and that calculated using the variable R_{surf} derived here, demonstrates the importance of precisely determining R_{surf} for the proper interpretation of marine $\Delta^{14}C$ records. We therefore suggest that accurately mapping the spatial and temporal variability of R_{surf} during the deglaciation should be a top priority for palaeoclimate studies.

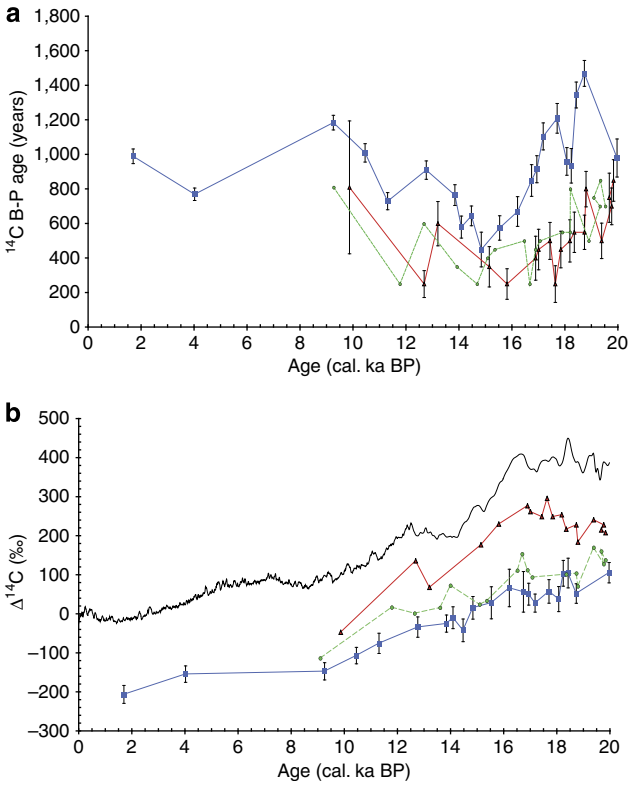

Figure 5 | South-Eastern Pacific waters ^{14}C activity. (**a**) Comparison between benthic–planktic radiocarbon age difference in core MD07-3088 (^{14}C B-P age; this study; blue squares) and core SO161-SL122 (red triangles[11]) and recalculated ^{14}C B-P age in core SO161-SL122 using the variable R_{surf} from this study (green circles). The error bars represent combined 1σ error in the ^{14}C dates. (**b**) Comparison of the atmospheric ^{14}C activity ($\Delta^{14}C$) from IntCal09 (black line) with oceanic ^{14}C activity ($\Delta^{14}C$) obtained from benthic foraminifera from core MD07-3088 (this study; blue squares), benthic foraminifera $\Delta^{14}C$ from intermediate waters off Chile from core SO161-SL122 after De Pol-Holz *et al.*[11] (red triangles) and recalculated using the variable R_{surf} from this study (green circles).

Methods

Study site. Calypso core MD07-3088 was collected during the IMAGES PACHIDERME (MD 159) expedition by the French R/V Marion Dufresne in the SEP (46°04 S; 075°41 W; 1536 m; 18.9 m length; Fig. 1). Coring at this site recovered a fairly uniform succession of olive black to greyish olive diatom and silt-bearing clay for the upper 6 m. For the remaining 12.9 m, the sediment is dominated by greyish olive to grey silty clay with intercalations of silty/sandy layers. In this study, the first 17 m of the core are presented.

The core location is within the ACC latitude belt under the direct influence of the northward Ekman transport of SSW (Fig. 1a,b (ref. 16)). Today, the study site is bathed by the upper layers of the nutrient-rich, oxygen-poor Pacific Central Waters at the boundary with the northward-flowing oxygen-rich AAIW.

Stable isotopes. Stable oxygen and carbon isotope ratios ($\delta^{18}O$, $\delta^{13}C$), expressed in ‰ versus VPDB (Vienna Pee Dee Belemnite standard) were obtained for the planktic foraminifera *G. bulloides* sampled every 5 cm. In addition, $\delta^{13}C$ measurements were performed on the benthic foraminifera *Cibicides wuellestorfii* with a sampling resolution along the core every 10 cm. Six to ten shells were picked within the 250 to 315 μm size ranges for the planktonic analysis, one to four shells for the benthic analysis. Prior to isotopic analyses, the samples were cleaned in methanol using an ultrasonic bath for a few seconds then heated under vacuum at 380 °C for 45 min. Analyses were performed at Laboratoire des Sciences du Climat et de l'Environnement on Finnigan Delta + and GV Isoprime mass spectrometers. VPDB is defined with respect to the NBS19 calcite standard[42]. The mean external reproducibility (1σ) of carbonate standards is ± 0.06‰ for $\delta^{18}O$ and ± 0.04‰ for $\delta^{13}C$; measured NBS18 is −23.2 ± 0.2‰ VPDB for $\delta^{18}O$ and − 5.0 ± 0.1‰VPDB for $\delta^{13}C$. The reproducibility for *C. wuellestorfii* and *G. bulloides* are 0.04 and 0.21‰ for $\delta^{18}O$ and 0.06 and 0.23‰ for $\delta^{13}C$, respectively. The poor reproducibility for *G. bulloides* is because of the low number of specimens analysed, which prevent smoothing of the seasonal variation of the *G. bulloides* isotopic signal. However, the three-point average smoothed curve presented is closer to the annual mean signal.

Sea surface temperatures. Summer SSTs were determined using planktic foraminifera assemblages. Each sieved sample (>150 μm fraction) was split into 300–1,000 individuals for identification and counting. The SSTs were calculated using the Modern Analogue Technique[43], a SO database[44] and the PaleoAnalogs software[45]. This method directly measures the difference between the faunal composition of a fossil sample and a modern database, and it identifies, for each fossil assemblage, the best modern analogues. Reliability of SSTs is estimated using a square chord distance test (dissimilarity coefficient) that represents the mean degree of similarity between the sample and the best 4–20 modern analogues. The calculated mean standard deviation of SST estimates observed in core MD07-3088 is ~1.5 °C during the last 20 ka.

Geochemistry. Marine ash layers were identified by the relative abundance of glass shards in core MD07-3088 as previously described[30]. Counting of glass shards from 210 samples was previously conducted on the detrital fraction every 10 cm along the core, with a resolution of 5 cm between 600 and 900 cm because of the

occurrence of several eruptions closely spaced in time. Additional counts at higher resolution (every 1 cm) in core MD07-3088 between 275 and 285 cm permitted the identification of a new tephra layer at 278–279 cm (Supplementary Fig. S2). Major-element analyses of individual glass shards were performed on CAMECA-SX 100 Electron Microprobe (EPMA-CAMPARIS) at the University Pierre et Marie Curie (UPCM, Paris VI).

Radiocarbon dates. ^{14}C dating was performed at UMS-ARTEMIS (Pelletron 3MV) AMS (CNRS-CEA Saclay, France) and at Keck Carbon Cycle Accelerator Mass Spectrometer facilities, University of California, Irvine. AMS ^{14}C measurements were performed on handpicked monospecific planktic and mixed benthic foraminifera in the size fraction $>150\,\mu m$. Twenty-four dates were obtained for monospecific planktic foraminifera *G. bulloides* and 22 were obtained for mixed benthic foraminifera. AMS ^{14}C results are provided in Supplementary Tables S1,S2.

The age model for the core was derived from the calibrated planktic ages by applying a variable R_{surf} correction (this study) and using the calibration program OxCal[25] at the 95% confidence level (2σ) based on IntCal09 (ref. 26) and IntCal04 (ref. 27). As this core has a very high sedimentation rate ($\sim$60 to 260 cm ka^{-1}), bioturbation effects should be minimal.

Finally, to compare the B-P foraminifera ^{14}C age of our core with the atmospheric ^{14}C history, we derived estimates of deep SEP $\Delta^{14}C$ by using the following equation[46]:

$$\Delta^{14}C = \left(\frac{e^{-\frac{^{14}C_{age}}{8,033}}}{e^{-\frac{calage}{8,266}}} - 1 \right) 1,000 \quad (1)$$

where 8,033 and 8,266 are the Libby and the true mean lives of ^{14}C, respectively. These values together with their 1σ uncertainties are listed in Supplementary Table S2.

Radiocarbon model simulation. To examine the influence of the changing atmospheric $\Delta^{14}C$ concentrations on the B-P ages at the location of core MD07-3088, we simulated the oceanic $\Delta^{14}C$ over the last 26 ka in a global ocean circulation model. For this simulation, we used a data-constrained circulation model[47], which has been fitted to modern hydrographic and tracer data. The model resolution is 2° in the horizontal with 24 unevenly spaced vertical levels. One of the model constraints is the pre-bomb radiocarbon concentration from the Global Ocean Data Analysis Project compilation[24]. The root mean squared model-data misfit for pre-bomb radiocarbon concentrations is 7.4‰, and the relative error is 0.7 (a value <1 indicates that the model-data misfit is within the estimated uncertainty of the observations).

We simulate $\Delta^{14}C$ over the deglaciation following the methodology of De Vries and Primeau[48]. We define the tracer $R = (\Delta^{14}C/1{,}000) + 1$, which is treated as a passive tracer that decays with an e-folding decay timescale of 8,266 years. Biological sources and sinks of R are neglected because their influence is small[49]. The only source of R in the ocean is because of gas exchange at the air–sea interface, where the flux of R is proportional to the atmospheric concentration R_{atm},

$$F = k(R_{atm} - R). \quad (2)$$

Following De Vries and Primeau[48], the piston velocity k is assumed to be proportional to the CO_2 piston velocity K_w,

$$k = K_w s \left(\frac{pCO_2}{DIC} \right) \quad (3)$$

where s is the solubility of CO_2 in seawater, pCO_2 is the partial pressure of atmospheric CO_2 and DIC is the mean surface dissolved inorganic carbon concentration. We use the CO_2 piston velocity from the Ocean Carbon Cycle Model Intercomparison Project Phase 2 protocol[50], which is reduced by a factor of 20% to account for recent estimates[51]. Atmospheric pCO_2 is prescribed to follow the reconstructed history from the EDC and Vostok ice cores[52]. DIC is assumed to change by 1% for every 10% change in atmospheric pCO_2, consistent with the average surface ocean buffer factor of $\sim$10 (ref. 53). Reference values for the pre-industrial period are $pCO_2 = 280\,\mu atm$ and DIC = 2 mmol m^{-3} (ref. 50). The solubility s is derived from modern temperature and salinity using the equation of Weiss[54]. Temporal variability in s is ignored because deglacial temperature and salinity records are sparse, and changes in s are likely to be smaller than the changes in pCO_2.

We perform two simulations; one in which the atmospheric history R_{atm} is taken from the IntCal09 reconstruction[26], and one in which we use R_{atm} from the IntCal04 reconstruction[27]. We then calculate the B-P age from the modelled surface and deep-ocean $\Delta^{14}C$ at the location of core MD07-3088. This B-P age record is the one that would be expected because of the observed changes in atmospheric $\Delta^{14}C$, if there were no changes in the ocean circulation. The difference then between the reconstructed B-P ages and the modelled B-P ages are due entirely to changes in circulation, having removed the influence of changing atmospheric $\Delta^{14}C$.

Radiocarbon and $\delta^{13}C$ as oceanographic tracers. The $\delta^{13}C$ of DIC and ^{14}C are both tracers of water masses. They are used together here as their distribution is not primarily controlled by the same factors. The $\delta^{13}C$ distribution is controlled by the action of biology, which preferentially strips ^{12}C out of surface waters by ocean circulation that brings nutrients back into surface waters and by the exchange of CO_2 between the atmosphere and the ocean. The impact of air–sea exchange on the $\delta^{13}C$ distribution depends on the rate of exchange and on the temperature of surface waters[55].

Biological and temperature fractionation effects are, however, negligible for the ^{14}C distribution, as they have very little effect compared with radioactive decay[49], which lends a strong vertical gradient to the ^{14}C age distribution. The common mechanism that can affect vertical distributions of both $\Delta\delta^{13}C$ and B-P ^{14}C age is oceanic vertical mixing: changes in the vertical gradient of $\Delta\delta^{13}C$ and B-P ^{14}C age that are relatively rapid, synchronous and in the same direction (such as those observed during the upwelling periods highlighted in Fig. 3) are therefore most likely caused by changes in vertical mixing rates.

References

1. Bard, E. *et al.* The North Atlantic atmosphere-sea surface ^{14}C gradient during the Younger Dryas climatic event. *Earth Planet. Sci. Lett.* **126,** 275–287 (1994).
2. Siani, G. *et al.* Mediterranean sea-surface radiocarbon reservoir age changes since the last glacial maximum. *Science* **294,** 1917–1920 (2001).
3. Sikes, E. L., Samson, C. R., Guilderson, T. P. & Howard, W. R. Old radiocarbon ages in the southwest Pacific Ocean during the last glacial period and deglaciation. *Nature* **405,** 555–559 (2000).
4. Toggweiler, J. R., Russell, J. L. & Carson, S. R. Midlatitude westerlies, atmospheric CO_2, and climate change during the ice ages. *Paleoceanography* **21,** 1–15 (2006).
5. Anderson, R. F. *et al.* Wind-driven upwelling in the Southern Ocean and the deglacial rise in atmospheric CO_2. *Science* **323,** 1443–1448 (2009).
6. Marchitto, T., Lehman, S., Ortiz, J., Fluckiger, J. & van Geen, A. Marine radiocarbon evidence for the mechanism of deglacial atmospheric CO_2 rise. *Science* **316,** 1456–1459 (2007).
7. Galbraith, E. *et al.* Carbon dioxide release from the North Pacific abyss during the last deglaciation. *Nature* **449,** 890–893 (2007).
8. Skinner, L. C., Fallon, S., Waelbroeck, C., Michel, E. & Barker, S. Ventilation of the deep Southern Ocean and deglacial CO_2 rise. *Science* **328,** 1147–1151 (2010).
9. Marshall, J. & Speer, K. Closure of the meridional overturning circulation through Southern Ocean upwelling. *Nat. Geosci.* **5,** 171–180 (2012).
10. Spero, H. J. & Lea, D. W. The cause of carbon isotope minimum events on glacial terminations. *Science* **296,** 522–525 (2002).
11. De Pol-Holz, R. *et al.* No signature of abyssal carbon in intermediate waters off Chile during deglaciation. *Nat. Geosci.* **3,** 192–195 (2010).
12. Stott, L., Southon, J., Timmermann, A. & Koutavas, A. Radiocarbon age anomaly at intermediate water depth in the Pacific Ocean during the last deglaciation. *Paleoceanography* **24,** 1–10 (2009).
13. Rose, K. A. *et al.* Upper-ocean-to-atmosphere radiocarbon offsets imply fast deglacial carbon dioxide release. *Nature* **466,** 1093–1097 (2010).
14. Muratli, J. M., Chase, Z., Mix, A. & McManus, J. Increased glacial-age ventilation of the Chilean margin by Antarctic intermediatewater. *Nat. Geosci.* **3,** 23–26 (2010).
15. Burke, A. & Robinson, L. F. The Southern Ocean's role in carbon exchange during the last deglaciation. *Science* **335,** 557–561 (2012).
16. Strub, P. T., Mesias, J. M., Montecino, V., Ruttlant, J. & Salinas, S. Coastal ocean circulation off Western South America in *The Global Coastal Ocean, Regional Studies and Syntheses.* 273–315 (Wiley, 1998).
17. Ingram, B. L. & Southon, J. R. Reservoir ages in Eastern Pacific coastal and estuarine waters. *Radiocarbon* **38,** 573–582 (1996).
18. Kilian, R. & Lamy, F. A review of glacial and holocene paleoclimate records from southernmost Patagonia (49-55°S), *Quat. Sci. Rev.* **53,** 1–23 (2012).
19. Van Beek, P. *et al.* 226Ra in barite: absolute dating of holocene Southern Ocean sediments and reconstruction of sea-surface reservoir ages. *Geology* **30,** 731–734 (2002).
20. Fontugne, M., Carré, M., Bentaleb, I., Julien, M. & Lavallée, D. Radiocarbon reservoir ages variations in the south peruvian upwelling during the Holocene. *Radiocarbon* **46,** 531–537 (2004).
21. Ortlieb, L., Vargas, G. & Saliège, J. F. Marine radiocarbon reservoir effect along the northern Chile-southern Peru coast (14–24°S) throughout the Holocene. *Quat. Res.* **75,** 91–103 (2011).
22. Hall, B. L., Henderson, G. M., Baroni, C. & Kellogg, T. B. Constant Holocene Southern-Ocean ^{14}C reservoir ages and ice-shelf flow rates. *Earth Planet. Sci. Lett.* **296,** 115–123 (2010).
23. Forsythe, R. D. *et al.* Pliocene near trench magmatism in southern Chile: a possible manifestation of ridge collision. *Geology* **14,** 23–27 (1986).
24. Key, R. *et al.* A global ocean carbon climatology: Results from Global Data Analysis Project (GLODAP). *Glob. Biogeochem. Cycles* **18,** 1–23 (2004).
25. Bronk Ramsey, C. Bayesian analysis of radiocarbon dates. *Radiocarbon* **51,** 337–360 (2009).
26. Reimer, P. J. *et al.* IntCal09 and Marine09 radiocarbon age calibration curves, 0–50,000 years cal BP. *Radiocarbon* **51,** 1111–1150 (2009).

27. Reimer, P. J. *et al.* Terrestrial radiocarbon age calibration, 0-26 cal kyr BP. *Radiocarbon* **46,** 1029–1058 (2004).
28. Southon, J. *et al.* A high-resolution record of atmospheric ^{14}C based on Hulu Cave speleothem H82. *Quat. Sci. Rev.* **33,** 32–41 (2012).
29. Bronk Ramsey, C. *et al.* A complete terrestrial radiocarbon record for 11.2 to 52.8 kyr B.P. *Science* **338,** 370–374 (2012).
30. Carel, M., Siani, G. & Delpech, G. Tephrostratigraphy of a deep-sea sediment sequence off the south Chilean margin: new insight on the Hudson volcanic activity since the last glacial period. *J. Volcanol. Geothermal. Res.* **208,** 99–111 (2011).
31. Glasser, N. F., Harrison, S., Winchester, V. & Aniya, M. Late Pleistocene and Holocene palaeoclimate and glacier fluctuations in Patagonia. *Global Planet. Change* **43,** 79–101 (2004).
32. Lourantou, A. *et al.* A detailed carbon isotopic constraint on the causes of the deglacial CO_2 increase. *Global Biogeochem. Cycles* **24,** 1–15 (2009).
33. Schmitt, J. *et al.* Carbon isotope constraints on the deglacial CO_2 rise from ice cores. *Science* **336,** 711–714 (2012).
34. Gherardi, J. M. *et al.* Glacial-interglacial circulation changes inferred from 231Pa/230Th sedimentary record in the North Atlantic region. *Paleoceanography* **24,** PA2204 (2009).
35. Monnin, E. *et al.* Atmospheric CO_2 concentrations over the last glacial termination. *Science* **291,** 112–114 (2001).
36. Lemieux-Dudon, B. *et al.* Consistent dating for Antarctic and Greenland ice cores. *Quat. Sci. Rev.* **29,** 8–20 (2010).
37. Stenni, B. *et al.* An oceanic cold reversal during the last deglaciation. *Science* **293,** 2074–2077 (2001).
38. Siani, G. *et al.* Late Glacial to Holocene terrigenous sediment record in the Northern Patagonian margin: Paleoclimate implications. *Paleogeogr. Paleoclimatol. Paleoecol.* **297,** 26–36 (2010).
39. Pedro, J. B., Rasmussen, S. O. & van Ommen, T. D. Tightened constraints on the time-lag between Antarctic temperature and CO_2 during the last deglaciation. *Clim. Past.* **8,** 1213–1221 (2012).
40. Parrenin, F. *et al.* On the gas-ice depth difference (Δdepth) along the EPICA Dome C ice core. *Clim. Past.* **8,** 1239–1255 (2012).
41. Parrenin, F. *et al.* Synchronous change of atmospheric CO_2 and antarctic temperature during the last deglacial warming. *Science* **339,** 1060–1063 (2013).
42. Coplen, T. B. Normalization of oxygen and hydrogen isotope data. *Chem. Geol.* **72,** 293–297 (1988).
43. Prell, W. The stability of low-latitude Sea-Surface Temperatures: an evaluation of the CLIMAP reconstruction with emphasis on the positive SST anomalies, *Tech. Rep. TR025*, 1-60 (U.S. Dept. of Energy, 1985).
44. Govin, A. *et al.* Evidence for northward expansion of Antarctic Bottom Water mass in the Southern Ocean during the last glacial inception. *Paleoceanography* **24,** PA1202 (2009).
45. Theron, R. *et al.* Rapid reconstruction of paleoenvironmental features using a new multiplatform program. *Micropaleontology* **50,** 391–395 (2004).
46. Adkins, J. F. & Boyle, E. A. Changing atmospheric 14C and the record of deep water paleo-ventilation ages. *Paleoceanography* **12,** 337–344 (1997).
47. DeVries, T. & Primeau, F. Dynamically- and observationally-constrained estimates of water-mass distributions and ages in the global ocean. *J. Phys. Oceanograph.* **41,** 2381–2401 (2011).
48. DeVries, T. & Primeau, F. An improved method for estimating water-mass ventilation Age from radiocarbon measurements. *Earth Planet. Sci. Lett.* **295,** 367–378 (2010).
49. Fiadeiro, M. E. Three-dimensional modeling of tracers in the deep Pacific Ocean, II, Radiocarbon and the circulation. *J. Mar. Res.* **40,** 537–550 (1982).
50. Najjar, R. & Orr, J. Design of OCMIP-2 simulations of chlorofuorocarbons, the solubility pump and common biogeochemistry, http://www.ipsl.jussieu.fr/OCMIP/phase2/simulations/design.ps (1998).
51. Sweeney, C. *et al.* Constraining global air-sea gas exchange for CO_2 with recent bomb ^{14}C measurements. *Global Biogeochem. Cycles* **21,** 1–10 (2007).
52. Luthi, D. *et al.* High-resolution carbon dioxide concentration record 650,000-800,000 years before present. *Nature* **453,** 379–382 (2008).
53. Bolin, B. & Eriksson, E. Changes in the carbon dioxide content of the atmosphere and sea due to fossil fuel combustion. in *The Atmosphere and the Sea in Motion*. (ed. Bolin, B.) 130–142 (Rockefeller Inst. Press, 1959).
54. Weiss, R. Carbon dioxide in water and seawater: the solubility of a non-ideal gas. *Mar. Chem.* **2,** 203–215 (1974).
55. Lynch-Stieglitz, J. *et al.* The influence of air-sea exchange on the isotopic composition of oceanic carbon: observations and modeling. *Global Biogeochem. Cycles* **21,** 653–665 (1995).
56. Schlitzer, R. Ocean Data View, http://odv.awi.de (2012).

Acknowledgements

Financial support for this study was provided by the French INSU/LEFE—Pachiderme project and the Chilean 'Fondecyt 11100281 /FONDAP 15110009'. This study has been conducted in the framework of the international IMAGES program and the MD159-PACHIDERME/IMAGES cruise. We express our thanks to the crew of the R/V Marion Dufresne as well as the French Polar Institute (IPEV). We also thank D. Paillard, M. Paterne, J.C. Duplessy and J. Southon for their helpful discussions. The LSCE contribution no. is 5,073.

Author contributions

G.S. and E.M. conceived the study and wrote the manuscript. G.S., E.M. and R.D.P.-H. performed radiocarbon dating, G.S. and G.I. counted planktic foraminifera assemblages and G.S and E.M. performed the statistical analyses for paleotemperatures estimations, E.M. and F.D. supervised stable isotope measurements, T.D. carried out model analysis and interpretation, G.S. and M.C. contributed to tephra study, R.D.P.-H., T.D., F.L. and A.L. also contributed to the data interpretation and discussion of the results.

Additional information

Supplementary Information accompanies this paper at http://www.nature.com/naturecommunications

Competing financial interests: The authors declare no competing financial interests.

Reprints and permission information is available online at http://npg.nature.com/reprintsandpermissions/

How to cite this article: Siani, G. *et al.* Carbon isotope records reveal precise timing of enhanced Southern Ocean upwelling during the last deglaciation. *Nat. Commun.* 4:2758 doi: 10.1038/ncomms3758 (2013).

Supplementary Information

Supplementary Figures

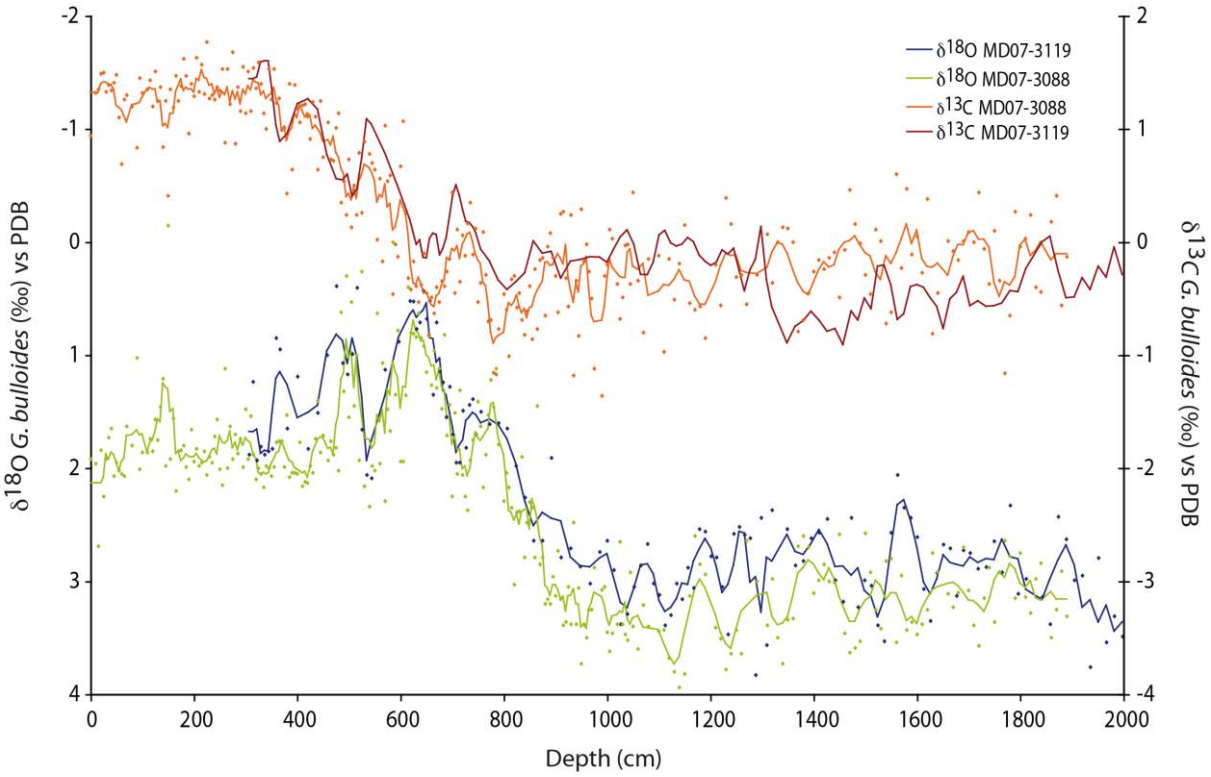

Supplementary Figure S1. Stable isotope records of *Globigerina bulloides*. Carbon ($\delta^{13}C$) and oxygen ($\delta^{18}O$) isotopic records from core MD07-3088 (this study) and nearby farther offshore core MD07-3119. Thick lines for oxygen and carbon isotope records correspond to the smoothed curve using a 3 point average.

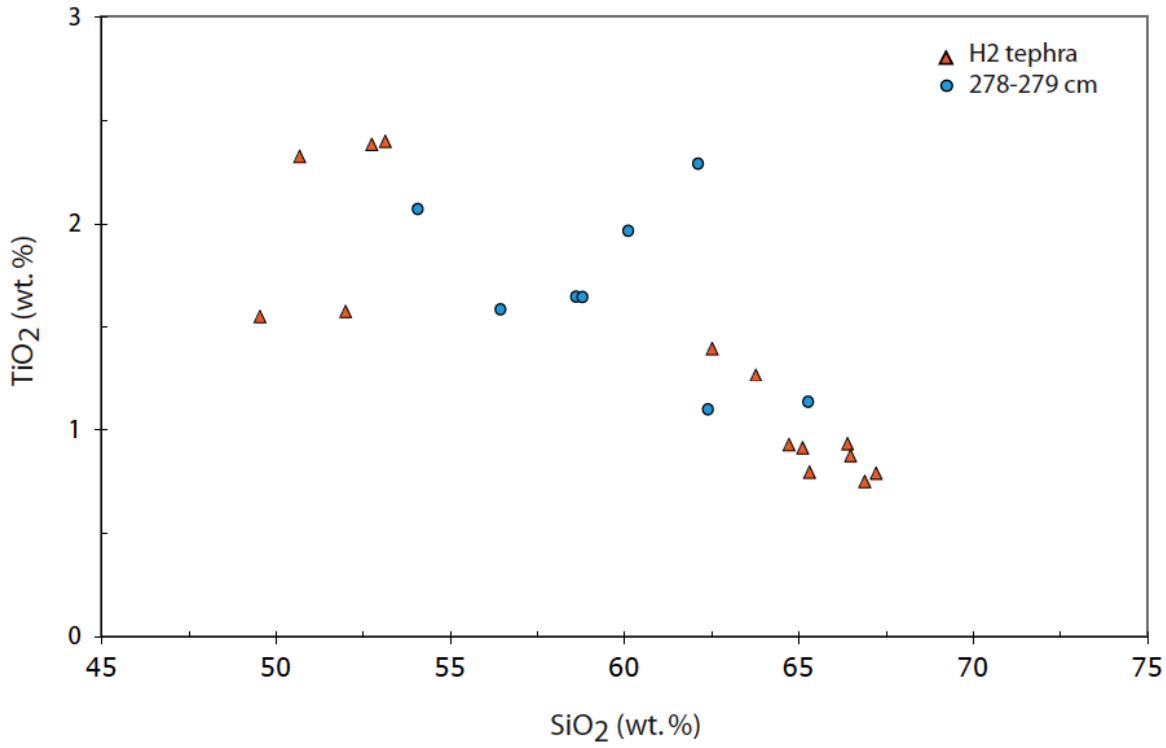

Supplementary Figure S2. Discrimination of the marine tephra volcanic source. TiO_2 vs. SiO_2 showing the correlation between cryptotephra layer at 278-279 cm in core MD07-3088 and on-land deposits of the H2 eruption attributed to the explosive activity of the Hudson volcano[57].

Supplementary Tables

Supplementary Table S1. Tephra ages and sea surface reservoir ^{14}C ages estimates in core MD07-3088 . Marine and terrestrial ^{14}C age results of the tephra recovered in core MD07-3088 and on the continent[57-58], eruption sources and reservoir age (R_{surf}) calculations. Terrestrial ^{14}C dating marked with an asterisk are from ref. 57. Dating in bold correspond to the weighted means and 1σ uncertainties. Reservoir age (R_{surf}) = marine ^{14}C age - terrestrial ^{14}C age. Conventional ^{14}C age, as defined by ref. 59. Calendar ages are calculated from ref. 25 and 26.

Marine Tephra depth (cm)	Marine samples	Marine conventional ^{14}C age (yr BP) ± 1σ	Terrestrial samples	Terrestrial conventional ^{14}C age (yr BP) ± 1σ	Eruption	Origin	R_{surf} (yr) ± 1σ	Calendar age (yr BP)
159-161	*Globigerina bulloides*	2510±30	Charcoal	1830±75	HW7	Hudson	790 ± 160	1695
			Charcoal	1605±55				
				1720±160				
280-281	*Globigerina bulloides*	4475±30	Peat	3740±60*	H2	Hudson	805 ± 140	4015
			Peat	3485±100*				
			Charcoal	3670±70*				
			Charcoal	3790±80*				
				3670±130				
660-661	*Globigerina bulloides*	10,880±35	Charcoal	9830±90	HW3	Hudson	920 ± 135	11470
			Charcoal	10,080±100				
			Charcoal	9995±85				
			Charcoal	9930±85				
				9960±105				
750-751	*Globigerina bulloides*	12,885±40	Charcoal	11,965±100	HW2	Hudson	975 ± 120	13840
			Charcoal	11,855±120				
				11,910±80				
800-801	*Globigerina bulloides*	13,755±35	Charcoal	12,390±120	HW1	Hudson	1320 ± 95	14465
			Charcoal	12,480±100				
				12,435±65				

Supplementary Table S2. Compiled radiocarbon data. Planktic and benthic radiocarbon dates, B-P offset and $\Delta^{14}C$ estimates from core MD07-3088.

Lab Code	Species	Depth (cm)	Conventional ^{14}C age (yr)	1 σ (yr)	B-P ages (yr)	1 σ (yr)	Calendar age (yr)	Upper limit (1 σ)	Lower limit (1 σ)	$\Delta^{14}C$ benthic (‰)	(1 σ)
SacA 10551	*Mix benthic*	0-3	1595	30						-180	23
SacA 10552	G.bulloides	159-161	2510	30	990	40	1695	190	180	-206	21
SacA 12814	*Mix benthic*	159-161	3500	30							
SacA 12815	G.bulloides	280-281	4475	30	770	35	4015	195	185	-154	19
UCIAM-S97354	*Mix benthic*	280-282	5245	20							
SacA 12816	G.bulloides	360-362	5975	35			5940	170	170		
SacA 12817	G.bulloides	500-501	8430	30			8435	175	155		
SacA 10553	G.bulloides	539-541	9080	30	1185	40	9250	155	185	-147	21
SacA 12818	*Mix benthic*	540-541	10265	30							
SacA 12819	G.bulloides	610-611	10050	35	1010	55	10450	210	180	-107	26
SacA 21652	*Mix benthic*	609-610	11060	40							
SacA 10554	G.bulloides	660-661	10880	35	730	50	11470	210	160	-75	26
SacA 21653	*Mix benthic*	660-661	11610	35							
SacA 21648	G.bulloides	700-701	11765	35	910	55	12760	165	135	-34	22
SacA 21654	*Mix benthic*	700-701	12675	40							
SacA 12820	G.bulloides	750-751	12885	40	765	60	13840	95	115	-25	28
SacA 21655	*Mix benthic*	750-751	13650	45							
SacA 21649	G.bulloides	780-781	13185	45	580	65	14085	225	165	-10	29
SacA 21656	*Mix benthic*	780-781	13765	45							
SacA 12821	G.bulloides	800-801	13755	35	645	60	14465	225	185	-42	29
SacA 21657	*Mix benthic*	800-801	14400	45							
UCIAM-S97349	G.bulloides	810-811	13840	45	450	100	14835	225	255	16	41
UCIAM-S97355	*Mix benthic*	810-811	14290	90							
UCIAM-S97350	G.bulloides	830-831	14290	50	575	70	15530	380	290	28	48
UCIAM-S97356	*Mix benthic*	830-831	14865	50							
UCIAM-S97351	G.bulloides	850-851	14560	50	670	85	16205	290	370	66	52
UCIAM-S97357	*Mix benthic*	850-851	15230	70							
SacA 12822	G.bulloides	870-871	14970	80	850	90	16735	145	195	56	28
SacA 12823	*Mix benthic*	870-871	15820	45							
UCIAM-S97352	G.bulloides	880-881	15145	50	915	80	16935	125	115	50	23
UCIAM-S97358	*Mix benthic*	880-881	16060	60							
SacA 21650	G.bulloides	900-901	15365	50	1105	80	17175	205	155	28	30
SacA 21658	*Mix benthic*	900-901	16470	60							
UCIAM-S97353	G.bulloides	940-941	15540	70	1210	85	17700	180	220	57	32
SacA 21659	*Mix benthic*	940-941	16750	50							
SacA 12824	G.bulloides	990-991	16295	50	960	115	18065	155	145	38	33
SacA 21660	*Mix benthic*	990-991	17180	60							
SacA 21662	Uvigerina	990-991	17330	60							
	Mean benthic		17255	106							
SacA 21651	G.bulloides	1020-1021	15990	50	935	155	18235	140	130	104	38
SacA 21663	Uvigerina	1020-1021	16820	50							
SacA 21664	*Mix benthic*	1020-1021	17030	50							
	Mean benthic		16925	150							
SacA 12825	G.bulloides	1040-1041	15755	45	1345	75	18420	105	145	105	25
SacA 21661	*Mix benthic*	1040-1041	17100	60							
SacA 10555	G.bulloides	1170-1172	16320	45	1470	75	18730	165	125	52	26
SacA 12826	*Mix benthic*	1170-1171	17790	60							
SacA 12827	G.bulloides	1710-1711	17610	50	980	110	19960	205	235	105	43
UCIAM-S97359	*Mix benthic*	1710-1711	18590	100							
SacA 12828	G.bulloides	1890-1891	18800	60			21415	280	320		

Supplementary References

57. Naranjo, J.A. & Stern, C.R. Holocene explosive activity of Hudson Volcano, southern Andes. *Bull. Volcanology*, **59**, 291-306 (1998).

58. Haberle, S.G. & Lumley, S.H. Age and origin of tephra recorded in postglacial lake sediments to the west of the southern Andes, 44 S to 47 S. *J. Volcanology Geothermal Res.* **84**, 239-256 (1998).

59. Stuiver, M. & Polach, H.A. Reporting of ^{14}C data. *Radiocarbon* **19**, 355–363 (1977).